ROOM TEMPERATURE FATIGUE RESPONSE OF γ-TiAl TO IMPACT DAMAGE

T. S. Harding[1], J. W. Jones,[1] P.S. Steif[2] and T.M. Pollock[3]

[1]Department of Materials Science and Engineering, University of Michigan, Ann Arbor, MI 48109-2136 USA [2]Department of Mechanical Engineering, Carnegie Mellon University, Pittsburgh, PA 15213 USA [3]Department of Materials Science and Engineering, Carnegie Mellon University, Pittsburgh, PA 15213 USA

Introduction

Gamma based titanium aluminides have received considerable attention recently as candidate materials in gas turbine applications, particularly low pressure turbine blades (1–3). Their low density and high specific stiffness, result in potentially significant weight savings in structures such as gas turbine engines if substituted for current materials. Two γ-TiAl microstructures are predominately identified in the literature: a lamellar microstructure consisting of alternating plates of γ and α_2, and a duplex microstructure consisting of equiaxed γ grains and lamellar colonies (3,4). Lamellar alloys generally exhibit better fracture toughness and fatigue crack growth resistance (5–7). Duplex alloys, on the other hand, exhibit superior ductility and tensile strength, but lower fatigue crack growth resistance (8). In both microstructures fatigue crack growth behavior is characterized by a strong dependence on cyclic stress intensity range, ΔK (5). This sensitivity can lead to very short lifetimes if initiation lifetime is negated by defects produced by foreign object or manufacturing-related impact damage.

The objective of the present study is to characterize and quantify the damage resulting from low-speed impacts on γ-TiAl and to relate this impact damage to reductions in fatigue failure stress by the use of a threshold-based model.

Materials and Experimental Procedure

A duplex alloy (48-2-2) with a composition of Ti-47.9A1-2.0Cr-1.9Nb (at.%) (9) and a lamellar alloy (WMS) with a composition of Ti-47.3A1-2.2Nb-0.5Mn-0.4W-0.4Mo-0.23Si (at.%) (10) were investigated. The 48-2-2 alloy was investment cast into plates that were heat treated in vacuum at 1093°C for 5 h. Hot isostatic pressing (HIP) at 1205°C and 172 MPa for 4 h was followed by a final heat treatment at 1205°C for 2 h and a rapid cool. This processing resulted in a final duplex microstructure, shown in Figure 1 (a), with a γ grain size of roughly 70 μm and approximately 6 vol% lamellar colonies. The WMS alloy was investment cast into plates that were processed with a HIP treatment at 1260°C and 172 MPa for 4 h, followed by a heat treatment of 1010°C for 50 h. The microstructure of this alloy, shown in Figure 1 (b), was nearly-fully lamellar with a lamellar colony size of 165 μm. Typical room
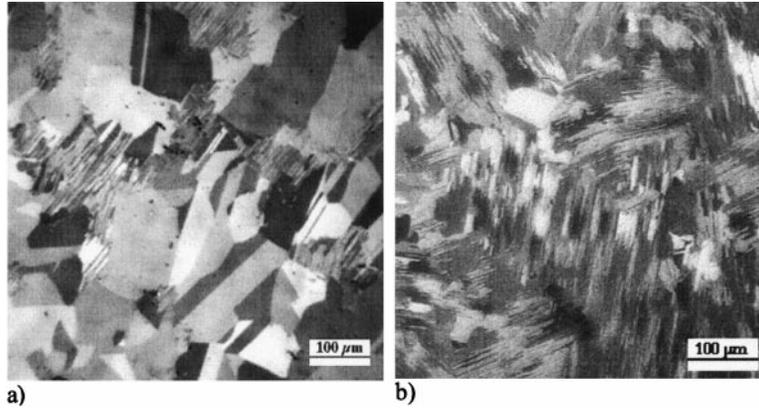
Figure 1. Microstructure of a) Duplex Ti-47.9A1-2.0Cr-1.9Nb alloy and b) Ti-47.3A1 2.2Nb-0.5Mn-0.4W-0.4Mo-0.23Si alloy.

temperature mechanical properties from electropolished specimens of both alloys are provided in Table 1.

Fatigue specimens were prepared from the cast plates by electro-discharge machining (EDM). Specimens were machined into rectangular dogbone shapes with a 136mm gage length and a 6mm × 3mm cross-section. Specimens were low stress ground, hand polished to a 600 grit finish and then electropolished in a solution of 60% methanol, 35% n-butanol and 5% perchloric acid at a temperature of −50°C and voltage of 25V.

Impact damage was simulated by indenting the specimen with a sharp, hardened steel wedge with a 60° flank angle using low speed "static" indents with an Instron testing machine. Each specimen was impacted or indented twice within the gage section with the same nominal peak impact load to produce two potential sites for fatigue failure.

Prior to cyclic loading damage was characterized by both optical and scanning electron microscope (SEM) methods. The damage parameters quantified are shown schematically in Figure 2. Here, effective crack length, a_{eff}, is defined here as the sum of the indent depth, D, and indent tip crack length, a, as described in Figure 2. In addition to this measure of damage, many isolated cracks were often observed throughout the plastic zone. These cracks were not typically connected to the indent, at least on the specimen surface.

Fatigue failure stress was determined using the step loading fatigue test method (11). In this approach, a specimen is tested for a predetermined number of cycles at each of a series of increasing stress levels until the specimen fails. In the present study, the cycle block size was 10^5 cycles and the maximum cyclic stress increment was 10 Mpa, with an initial stress that is approximately 75% of the predicted threshold stress. All tests were conducted on a servo-hydraulic fatigue test machine at room temperature in air. Tests were run at a frequency of 20Hz and with a constant load ratio of R = 0.1.

TABLE 1
Room Temperature Properties of a Duplex and Lamellar γ-TiAl Alloy

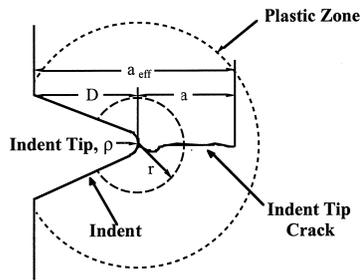| Property	Duplex "48-2-2"	Lamellar "WMS"
Yield Strength (MPa)	308	530
Tensile Strength (MPa)	384	580
Elongation (%)	1.1	0.9
Toughness (Mpa$\sqrt{}$m) (10)	24	1.9

Figure 2. Schematic diagram of damage zone from impact damage simulated by a 60° wedge shaped indenter.

Results and Discussion

The damage zone of a high severity impact (3100 N) in the 48-2-2 alloy is shown in Figure 3(a). The indent tip crack is primarily transgranular in nature, but in some specimens the crack initiated intergranularly from the indent tip when a properly aligned grain boundary was present at the indent tip. Figure 3(b) shows the damage zone of a high severity impact (2946 N) in the WMS alloy. Indent tip cracks in the lamellar microstructure of the WMS were primarily translamellar with some indications of interlamellar fracture.

Figure 4 compares the level of impact damage in terms of indentation depth and effective crack length with impact severity (peak impact load). From the figure, it can be shown that indent depth follows a linear relationship with peak impact load for both alloys. However, under the same impact load the depth of the indent in the 48-2-2 alloy is deeper due to the lower yield strength of this alloy. The effective crack length when compared with the depth of indentation is a measure of the extent of cracking ahead of the indent tip. From Figure 4 the formation of cracks occurs at a lower peak impact load in the 48-2-2 alloy (1000 N) compared to the WMS alloy (1600 N). However, these two critical peak impact loads result in very similar indent depths ($\sim$100 μm) in the two materials, suggesting that the extent of cracking ahead of the indent is controlled by the indent depth, and thus damage zone geometry, rather than peak impact load.

The high sensitivity of fatigue crack growth rate to stress intensity, common to γ-TiAl alloys, suggests that if the cyclic threshold stress intensity is exceeded the specimen should fail within a
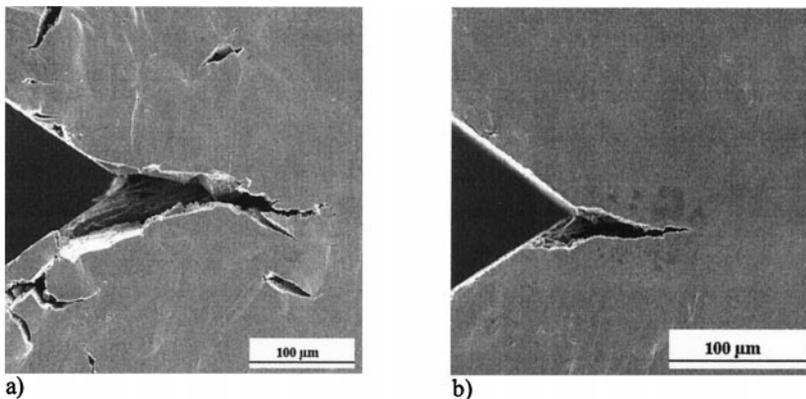

Figure 3. Indent tip cracks following high severity impacts in the a) 48-2-2 alloy (Peak Impact Load: 3100 N) and b) WMS alloy (Peak Impact Load: 2946 N).
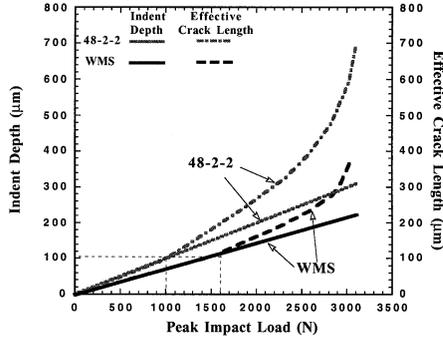
Figure 4. Correlation between peak impact load and the critical damage parameters for both the 48-2-2 alloy and WMS alloy.

relatively small number of cycles. In terms of the step test technique, when the stress level exceeds that of the predicted threshold stress, the specimen should fail within that cycle block or the next. Therefore, the predicted threshold stress and failure stress from the step test should be reasonably similar.

The predicted threshold stress for a specimen with an initial effective crack length, a_{eff}, can be determined using the simple LEFM calculation of equation (1).

$$\sigma_{TH} = \left(\frac{\Delta K_{TH}}{(1 - R)\, F\left(\dfrac{a_{eff}}{W} \right)\, \sqrt{\pi a_{eff}}} \right) \tag{1}$$

where ΔK_{TH} is the maximum cyclic threshold stress intensity determined from long crack growth data and W is the specimen width. Room temperature ΔK_{TH} values for 48-2-2 and WMS alloys are 6.9 MPa$\sqrt{}$m and 7.1 MPa$\sqrt{}$m respectively (12).

The reduction in fatigue failure stress caused by impact damage was correlated with the effective crack length using an approach modified from that of Kitagawa and Takahashi (13). Figure 5 compares the fatigue failure stress of both the 48-2-2 and WMS alloy to the effective crack length. From the plot it can be seen that when the effective crack length exceeds a transitional value the fatigue failure stress can be reasonably predicted using a threshold based approach. This is true for both alloys. However, what is significant is that the transitional flaw size for the WMS alloy is only 40 μm compared to 100 μm for the 48-2-2 alloy. Furthermore, at very severe damage levels, the fatigue failure stress of the 48-2-2 and WMS alloys are nearly the same. Thus, despite a greater fatigue strength in the undamaged
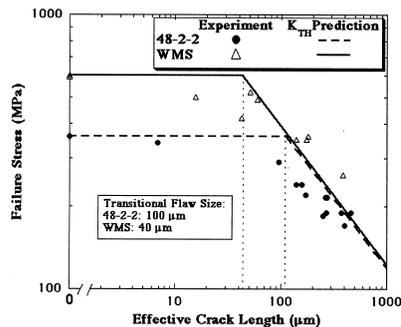

Figure 5. Comparison of the modified Kitagawa plots of the 48-2-2 and WMS alloys.

condition, the WMS alloy can withstand less damage before experiencing a reduction in fatigue strength and has little or no advantage in strength compared to the 48-2-2 alloy when damage is severe.

The failure stress for undamaged material was also established using the step test method, and was determined to be 360 MPa and 595 MPa for the 48-2-2 and WMS alloys respectively. For damage below the transitional flaw size, the threshold-based prediction becomes increasingly non-conservative as the failure stress approaches the fatigue failure stress for undamaged material.

Conclusions

1. For the alloys investigated, at damage levels greater than the transitional flaw size, the fatigue strength can be predicted using a threshold-based approximation. Below this transitional flaw size, the fatigue strength approaches that of the undamaged material.
2. The lamellar WMS γ-TiAl alloy suffers reduced fatigue strength at lower damage levels than does the duplex 48-2-2 alloy, and the two alloys have nearly the same fatigue strengths at severe damage levels.
3. The extent of impact damage, quantified by D and a_{eff} correlates best with peak impact load for both the 48-2-2 γ-TiAl and WMS γ-TiAl alloys.

Acknowledgement

References

1. C. M. Austin and T. J. Kelly, in Structural Intermetallics, ed. R. Darolia et al., p. 143, TMS, Warrendale, PA (1993).
2. J. M. Larsen, B. D. Worth, S. J. Balsone, and J. W. Jones, in Gamma Titanium Aluminides, ed. Y.-W. Kim, et al., p. 821, TMS, Warrendale, PA (1995).
3. S. C. Huang and J. C. Chesnutt, in Intermetallic Compounds: Vol. 2, Practice, ed. J. H. Westbrook and R. L. Fleischer, p. 73, Chichester, New York (1994).
4. K. S. Chan, J. Metals. 44, 30 (1992).
5. S. J. Balsone, J. M. Larsen, D. C. Maxwell, and J. W. Jones, Mater. Sci. Eng. A. A192/193, 457 (1995).
6. B. D. Worth, J. M. Larsen, S. J. Balsone, and J. W. Jones, Metall. Trans. A. 28, 825 (1997).
7. K. T. Venkataswara Rao, Y.-W. Kim, C. L., Muhlstein, and R. O. Ritchie, Mater. Sci. Eng. A. A192/193, 474 (1995).
8. J. Kumpfert, Y.-W. Kim, and D. M. Dimiduk, Mater. Sci. Eng. A. A192/1935 465 (1995).
9. S. C. Huang, General Electric Aircraft Engines, U.S. Patent 5,076,858 (1991).
10. P. R. Bowhal, H. F. Merrick, and D. E. Larsen, Jr., Mater. Sci. Eng. A. 192/193, 685 (1995).
11. J. A. Collins, Failure of Materials in Mechanical Design, John Wiley and Sons, New York (1993).
12. Data courtesy of A. H. Rosenberger, Wright Patterson Air Force Base (1998).
13. H. Kitagawa and S. Takahashi, in Proceedings of the 2nd International Conference on Mechanical Behavior in Metals, Boston, MA, p. 627, Pergamon Press, New York (1976).